GRIDLESS METHOD FOR UNSTEADY VISCOUS FLOWS

Pu Saihu, Chen Hongquan

(College of Aerospace Engineering, Nanjing University of Aeronautics and Astronautics, Nanjing, 210016, P. R. China)

Abstract: Gridless method is developed for unsteady viscous flows involving moving boundaries. The point distribution of gridless method is implemented in an isotropic or anisotropic way according to the features of viscous flows. In the area far away from the body, the traditional cloud of isotropic points is used, while in the adjacent area, the cloud of anisotropic points is distributed. In this way, the point spacing normal to the wall can be small enough for simulating the boundary layer, and meanwhile, the total number of points in the computational domain can be controlled due to large spacing in other tangential direction through the anisotropic way. A fast moving technique of clouds of points at each time-step is presented based on the attenuation law of disturbed motion for unsteady flows involving moving boundaries. In the mentioned cloud of points, a uniform weighted least-square curve fit method is utilized to discretize the spatial derivatives of the Navier-Stokes equations. The proposed gridless method, coupled with a dual time-stepping method and the Spalart-Allmaras turbulence model, is implemented for the Navier-Stokes equations. The computational results of unsteady viscous flows around a NLR7301 airfoil with an oscillating flap and a pitching NACA0012 airfoil are presented in a good agreement with the available experimental data.

Key words: gridless method; cloud of points; Navier-Stokes equations; unsteady flow; viscous flow

CLC number: V211.3 **Document code**: A **Article ID**: 1005-1120(2012)01-0001-08

INTRODUCTION

Gridless method using clouds of points without requirement for a grid has become one of the hottest research areas in computational fluid dynamics. This new kind of numerical method provides another choice to solve partial differential equations besides mesh methods. It has also been used for simulating steady flows over complex boundaries[1-4].

Unsteady flows, such as deployment of high lift devices, deflection of control surfaces, and flutter of the wing, are very common in aeronautical area as well as steady flows. In recent years, many researches have focused on gridless method for unsteady flows simulation. Kirshman, et al[5] combined a Cartesian mesh and gridless boundary conditions with application to flutter prediction. Wang, et al[6] developed a gridless method for unsteady inviscid flow simulation. Wang, et al[7] introduced a new dynamic cloud method based on Delaunay graph mapping strategy. These previous studies were mainly concerned on unsteady invicsid flows.

However, for many aeronautical applications, the unsteady flows should not be viewed as invicsid because the computing results can not agree with the experimental data. On the contrary, they are viscous. Based on this knowledge, a novel gridless method is developed to solve unsteady viscous flows with moving boundaries. The present work includes three main aspects: (1) How to generate the point distribution for viscous flows simulation, (2) How to get the point distribution at each time-step since the boundary is moving, (3) How to discretize the spatial derivatives and temporal derivatives of the Navier-Stokes (NS) equations on the obtained points. To answer the first question, a hybrid

Foundation items: Supported by the National Natural Science Foundation of China(10372043,11172134); the Funding of Jiangsu Innovation Program for Graduate Education(CXZZ11_0192).

Received date: 2011-01-14; **revision received date**: 2011-03-10

E-mail: hqchenam@nuaa.edu.cn

point distribution strategy is proposed by considering the features of viscous flows. A fast moving technique of clouds of points at every time step is presented based on the attenuation law of disturbed motion aiming at the moving boundaries. The spatial derivatives of flow quantities are evaluated at each point with a weighted least-square curve fit method in its cloud of points. A 2-D unsteady compressible NS code is developed by incorporating all the above ideas with the dual time-stepping procedure. The code is validated by simulating the viscous flows passing a NLR7301 airfoil with an oscillating flap and a pitching NACA0012 airfoil. The numerical results are also presented.

1 GOVERNING EQUATIONS

The governing equations of the study are the compressible NS equations in Cartesian coordinates. The equations are written in the non-dimensional form[8] as

$$\frac{\partial \boldsymbol{W}}{\partial t}+\frac{\partial \boldsymbol{E}}{\partial x}+\frac{\partial \boldsymbol{F}}{\partial y}-\left(\frac{\partial \boldsymbol{E}_{\mathrm{V}}}{\partial x}+\frac{\partial \boldsymbol{F}_{\mathrm{V}}}{\partial y}\right)=0 \tag{1}$$

The NS equations are non-dimensionalized by free stream density ρ_∞, free stream pressure p_∞, reference length L, and viscosity $\mu_\infty(Re_\infty/(\sqrt{\gamma}\cdot Ma_\infty))$ where Re_∞ and Ma_∞ represent the Reynolds number and Mach number of free stream. In Eq. (1), $\boldsymbol{W}$ is the vector of conservative variables, $\boldsymbol{E}$ and $\boldsymbol{F}$ the convective flux terms, $\boldsymbol{E}_{\mathrm{V}}$ and $\boldsymbol{F}_{\mathrm{V}}$ the viscous flux terms. The vector of conservative variables and the convective flux terms are given

$$\begin{aligned}\boldsymbol{W}&=[\rho,\rho u,\rho v,\rho e]^{\mathrm{T}}\\ \boldsymbol{E}&=[\rho U,\rho uU+p,\rho vU,\rho HU+x_t p]^{\mathrm{T}}\\ \boldsymbol{F}&=[\rho V,\rho uV,\rho vV+p,\rho HV+y_t p]^{\mathrm{T}}\end{aligned} \tag{2}$$

where ρ, p, e are the density, pressure, and total energy per unit mass, respectively, u and v the Cartesian components of velocity vector, $x_t=\mathrm{d}x/\mathrm{d}t$ and $y_t=\mathrm{d}y/\mathrm{d}t$ the moving velocity components of the point, where $\mathrm{d}x$, $\mathrm{d}y$ are the displacements of the point during the interval of time $\mathrm{d}t$, $U=u-x_t$, $V=v-y_t$. For a perfect gas, the total energy per unit volume is

$$\rho e=\frac{p}{\gamma-1}+\frac{1}{2}\rho(u^2+v^2) \tag{3}$$

where γ is the ratio of specific heats of the fluid and typically set as $\gamma=1.4$ for air.

The viscous flux terms $\boldsymbol{E}_{\mathrm{V}}$ and $\boldsymbol{F}_{\mathrm{V}}$ are given

$$\begin{aligned}\boldsymbol{E}_{\mathrm{V}}&=[0,\tau_{xx},\tau_{yx},\Theta_x]^{\mathrm{T}}\\ \boldsymbol{F}_{\mathrm{V}}&=[0,\tau_{xy},\tau_{yy},\Theta_y]^{\mathrm{T}}\end{aligned} \tag{4}$$

where the viscous stress are

$$\begin{aligned}\tau_{xx}&=\frac{2}{3}(\mu_{\mathrm{L}}+\mu_{\mathrm{T}})\left(2\frac{\partial u}{\partial x}-\frac{\partial v}{\partial y}\right)\\ \tau_{yy}&=\frac{2}{3}(\mu_{\mathrm{L}}+\mu_{\mathrm{T}})\left(2\frac{\partial v}{\partial y}-\frac{\partial u}{\partial x}\right)\\ \tau_{xy}&=\tau_{yx}=(\mu_{\mathrm{L}}+\mu_{\mathrm{T}})\left(\frac{\partial u}{\partial y}+\frac{\partial v}{\partial x}\right)\end{aligned} \tag{5}$$

$$\Theta_x=u\tau_{xx}+v\tau_{xy}+\frac{\gamma}{\gamma-1}\left(\frac{\mu_{\mathrm{L}}}{Pr_{\mathrm{L}}}+\frac{\mu_T}{Pr_{\mathrm{T}}}\right)\frac{\partial}{\partial x}\left(\frac{P}{\rho}\right)$$

$$\Theta_y=u\tau_{xy}+v\tau_{yy}+\frac{\gamma}{\gamma-1}\left(\frac{\mu_{\mathrm{L}}}{Pr_{\mathrm{L}}}+\frac{\mu_{\mathrm{T}}}{Pr_{\mathrm{T}}}\right)\frac{\partial}{\partial y}\left(\frac{P}{\rho}\right)$$

where μ_{L} is the laminar viscosity coefficient which is computed with the Sutherland formula and μ_{T} the turbulence viscosity coefficient which is obtained from the Spalart-Allmaras turbulence model[9]. The Euler equations are obtained by setting the viscous fluxes equal to zero.

2 POINT DISTRIBUTION AND MOVING TECHNIQUE FOR CLOUD OF POINTS

In gridless method, the spatial derivatives of the governing equations are discretized in the cloud of points. Since viscous flows are simulated, the point distribution is implemented in an isotropic or anisotropic way according to the features of viscous flows. In the area far away from the body, the traditional cloud of isotropic points[2-3] (Fig. 1(a)) is used, while in the adjacent area, the cloud of anisotropic points (Fig. 1(b)) is distributed. In this way, the point spacing normal to the wall is small enough for simulating the boundary layer while the total number of points in the computational domain is controlled due to the large spacing in other tangential direction through the anisotropic way.

Fig. 2 shows the point distribution around a NACA0012 airfoil obtained in the above way. This point distribution follows specific steps as: First, the airfoil and its wake region are wrapped in an envelope of points using the advancing-layers method[10] and the four neighboring points of

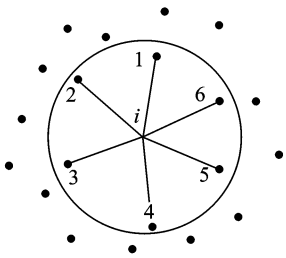

(a) Cloud of isotropic points

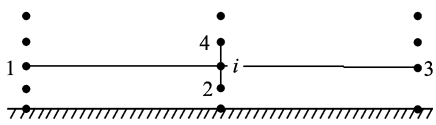

(b) Cloud of anisotropic points

Fig. 1 Cloud $C(i)$ for point i

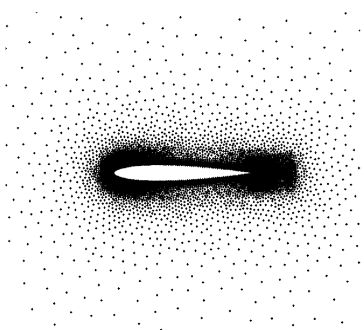

(a) Global view

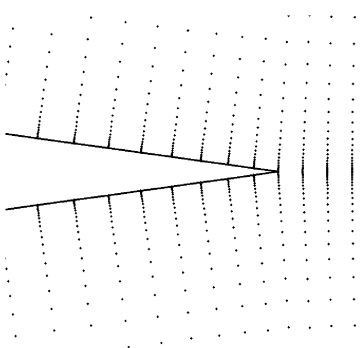

(b) Close-up view at trailing edge

Fig. 2 Point distribution around NACA0012 airfoil

each point obtained in this step are defined according to the layer structure (Fig. 1(b)). Second, the remaining part of the flow field is filled with points by delaunay triangulation[11] and the neighboring points of each point obtained in this step are also defined (Fig. 1(a)). It is obvious that when the advancing-layers method is implemented, the spacing normal to the wall can be easily controlled. In Fig. 2, the first point spacing normal to the wall is specified at 5×10^{-5}.

In unsteady flow computation, that clouds of points can move with the body boundaries is required to simulate the relative movement of body boundaries. Hence, a fast moving technique of clouds of points is used. The technique first proposed by Lu[12] for the dynamic structured grids is based on the attenuation law of disturbed motion. Here the technique is developed for the dynamic cloud of points by some modifications. The details of the technique are described as follows by taking the incompressible potential flow round a cylinder for example.

The stream function is

$$\psi = V_\infty\left(r - \frac{a^2}{r}\right)\sin\theta \tag{6}$$

where a is the radius of the cylinder, V_∞ the velocity of free stream. Magnify the cylinder's radius to $a+\varepsilon$, then the previous streamline passing point (r,θ) yields a normal displacement Δr

$$\Delta r = \varepsilon - \varepsilon\cdot\frac{(r-a)^2}{r^2+a^2} \tag{7}$$

It is difficult to generate dynamic grids using Eq. (7) directly. By further simplification, the coordinates (represented by subscript t) of the dynamic grids are

$$\boldsymbol{x}_t = \boldsymbol{x}_r - (\boldsymbol{x}_r - \boldsymbol{x}_s)\cdot g \tag{8}$$

where subscript r is the instantaneous coordinate which the static grids move to with bodies, s the boundary-fitted static grids used as initial values, g the function for the serial number of the grid line

$$g = \max\left(\left(\frac{i-i_b}{i_f-i_b}\right)^2, \left(\frac{j-j_b}{j_f-j_b}\right)^2\right) \tag{9}$$

where i, j are the serial numbers of each point. "b" is the corresponding boundary points and "f" the far field points. In the method, the new coordinates of each grid point are obtained directly by Eq. (8) without iteration. It is an efficient way for grid point moving. In fact, the method was successful in generating dynamic structured grids for the control surface moving and the wing flutter[8]. There is no serial number of each point in gridless method as that in structured grid, so Eq. (9) can not work in gridless method. Therefore, g is changed into

$$g = \left(\frac{d_f}{d+d_f}\right)^2 \tag{10}$$

where d is the distance between point i and the surface of the body, d_f the distance between point i and the far-field boundary. When the body moves, the new coordinates of each gridless point are also obtained directly by Eq. (8), and for each point, the topology of its clouds is not changed. Fig. 3 shows the point distribution when the airfoil rotates 30° about 25% of the chord on the basis of Fig. 2. The moving scale of the surface is very large but the point distribution mainly keeps the same quality as that of the initial point distribution adjacent to the wall, which profits the simulation of the boundary layer.

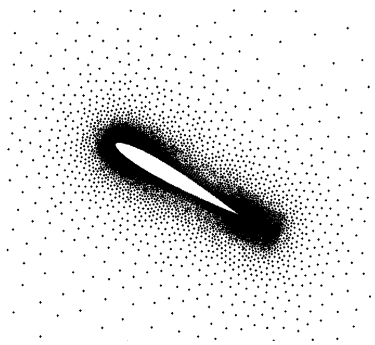

(a) Global view

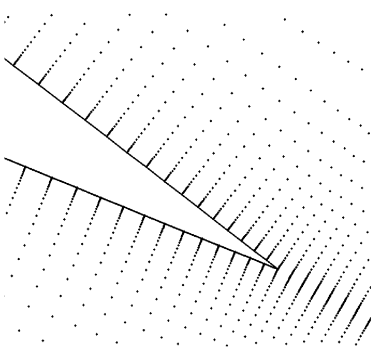

(b) Close-up view at trailing edge

Fig. 3 Point distribution around NACA0012 airfoil after rotating

3 NUMERICAL DISCRETIZATION OF GOVERNING EQUATIONS

3.1 Spatial discretization

For gridless method, the spatial derivatives of any quantities are evaluated through linear combinations of certain coefficients and the quantity of the cloud of points. For example, in the cloud of points $C(i)$ (Fig. 1), the first spatial derivatives of function f at point i are evaluated with the following linear combination forms[2]

$$\left.\frac{\partial f}{\partial x}\right|_i = \sum_{k=1}^{m} \alpha_{ik} f_{ik}$$
$$\left.\frac{\partial f}{\partial y}\right|_i = \sum_{k=1}^{m} \beta_{ik} f_{ik} \tag{11}$$

where m is the number of neighboring points of point i in the cloud of $C(i)$, and f_{ik} the value at the midpoint between points i and k. The coefficients α_{ik} and β_{ik} are obtained with a weighted least-squares curve fit to the following linear equation[4]

$$f = a + bx + cy \tag{12}$$

The weight functions used in this study are

$$w_{ik} = \left(\frac{\overline{r_i}}{r_k}\right)^2 \tag{13}$$

where r_k is the relative distances defined as

$$r_k = \sqrt{(x_k - x_i)^2 + (y_k - y_i)^2} \tag{14}$$

where $\overline{r_i}$ is set as the distance between the central point to the nearest point in its cloud of points.

Eq. (11) is applied to the convective flux of the NS equations to obtain the following expression

$$\frac{\partial \boldsymbol{E}}{\partial x} + \frac{\partial \boldsymbol{F}}{\partial y} = \sum_{k=1}^{m} (\alpha_{ik}\boldsymbol{E}_{ik} + \beta_{ik}\boldsymbol{F}_{ik}) = \sum_{k=1}^{m} \boldsymbol{G}_{ik} \tag{15}$$

The numerical flux $\boldsymbol{G}_{ik}$ at the midpoint between points i and k is obtained using Roe′s approximate Riemann solver[2].

The viscous terms of the NS equations are evaluated at each point

$$\left.\frac{\partial}{\partial x}\left(\mu \frac{\partial u}{\partial x}\right)\right|_i = \left.\frac{\partial \mu}{\partial x}\right|_i \cdot \left.\frac{\partial u}{\partial x}\right|_i + \mu_i \cdot \left.\frac{\partial}{\partial x}\left(\frac{\partial u}{\partial x}\right)\right|_i \tag{16}$$

where the first spatial derivatives is obtained by Eq. (11) directly, while the second derivative is obtained by

$$\left.\frac{\partial}{\partial x}\left(\frac{\partial u}{\partial x}\right)\right|_i = \sum_{k=1}^{m} \alpha_{ik} \left(\frac{\partial u}{\partial x}\right)_{ik} \tag{17}$$

The first derivative at the midpoint between points i and k is obtained as[4]

$$\left(\frac{\partial u}{\partial x}\right)_{ik} = \frac{\Delta x}{\Delta s^2}(u_k - u_i) +$$
$$\frac{1}{2}\frac{\Delta y}{\Delta s^2}\left(\Delta y\left(\left.\frac{\partial u}{\partial x}\right|_i + \left.\frac{\partial u}{\partial x}\right|_k\right) - \Delta x\left(\left.\frac{\partial u}{\partial y}\right|_i + \left.\frac{\partial u}{\partial y}\right|_k\right)\right) \tag{18}$$

where Δx, Δy, and Δs^2 are given as

$$\Delta x = x_k - x_i, \quad \Delta y = y_k - y_i$$
$$\Delta s^2 = \Delta x^2 + \Delta y^2 \tag{19}$$

After the spatial discretization, the semi-discretization form of the NS equations on point i is

$$\left.\frac{\partial \boldsymbol{W}}{\partial t}\right|_i + \boldsymbol{R}_i = 0 \tag{20}$$

3.2 Temporal discretization

Second-order backward difference method is implemented to the temporal derivatives of Eq. (20) as

$$\frac{3\boldsymbol{W}_i^{n+1} - 4\boldsymbol{W}_i^n + \boldsymbol{W}_i^{n-1}}{2\Delta t} + \boldsymbol{R}_i(\boldsymbol{W}_i^{n+1}) = 0 \tag{21}$$

where Δt is the global physical time step. A time-stepping methodology[13] is used to solve Eq. (21) to form the derivative term of conserved variables with respect to pseudo-time τ

$$\frac{\partial \boldsymbol{W}_i^{n+1}}{\partial \tau} + \frac{3\boldsymbol{W}_i^{n+1} - 4\boldsymbol{W}_i^n + \boldsymbol{W}_i^{n-1}}{2\Delta t} + \boldsymbol{R}_i(\boldsymbol{W}_i^{n+1}) = 0 \tag{22}$$

The unsteady residual is defined as

$$\boldsymbol{R}_i^*(\boldsymbol{W}_i^{n+1}) = \frac{3\boldsymbol{W}_i^{n+1} - 4\boldsymbol{W}_i^n + \boldsymbol{W}_i^{n-1}}{2\Delta t} + \boldsymbol{R}_i(\boldsymbol{W}_i^{n+1}) \tag{23}$$

Eq. (22) is reformed as

$$\frac{\partial \boldsymbol{W}_i^{n+1}}{\partial \tau} + \boldsymbol{R}_i^*(\boldsymbol{W}_i^{n+1}) = 0 \tag{24}$$

Then, the four-stage Runge-Kutta algorithm is used to solve Eq. (24) with the local time-stepping and residual averaging for accelerating[13]. For the viscous flows, no-slip boundary condition is imposed on the wall. In the far field, one dimensional characteristic analysis based on Riemann invariants is used to determine the values of the flow variables on the outside of the boundaries in the computational domain.

4 NUMERICAL RESULTS

In this section, the accuracy of the presented spatial discretization is firstly evaluated by the steady flow calculation on subsonic and transonic viscous flows around a NACA0012 airfoil. Then the unsteady flows around a NLR7301 airfoil with an oscillating flap and a pitching NACA0012 airfoil are simulated respectively.

4.1 Steady viscous flow around NACA0012 airfoil

Viscous flows over a NACA0012 airfoil were experimentally studied by Thibert et al[14]. To validate the present gridless method two test cases with different conditions are conducted: one is obtained at a free stream with Mach number of 0.5, an attack angle of 3.51°, and the Reynolds number of 2.93×10^6 (Fig. 4(a)), the other is obtained at a free stream with Mach number of 0.754, an attack angle of 3.02°, and the Reynolds number of 3.76×10^6 (Fig. 4(b)). The obtained pressure distributions on the airfoil surface are compared with the experimental data (Fig. 4), which indicates a good agreement between the numerical results of the proposed gridless solver and the experimental data. And from the view of these two cases, the accuracy of the present spatial discretization method is satisfactory.

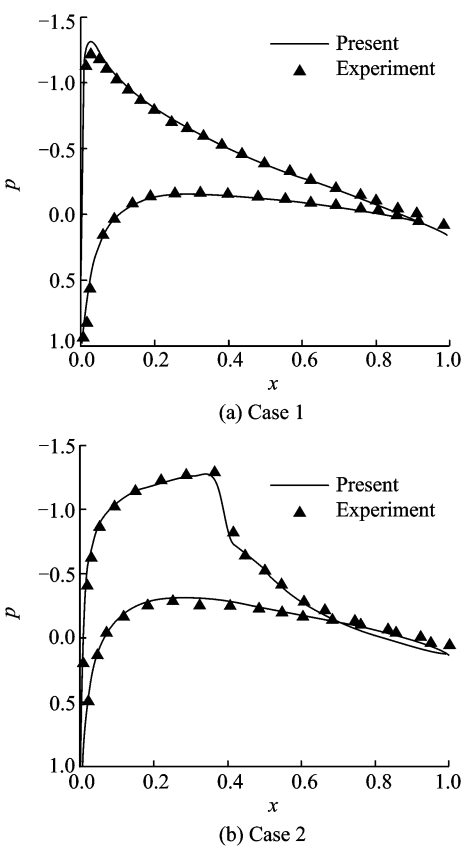

Fig. 4 Surface pressure comparisons

4.2 Unsteady viscous flow around NLR7301 airfoil with oscillation flap

The test of the unsteady viscous flow around

a NLR7301 airfoil is conducted. The part of airfoil surface before 75% of the chord stands still while the other part has an oscillation flap. The axis of the flap is located at 75% of the chord, the angle is set as $\delta(t)=0.03°+0.97°\sin(\omega t)$, and the reduced frequency is $k=\omega c/2U_\infty=0.071$, where c represents the chord length and U_∞ the free stream velocity. The free stream Mach number is 0.701, the attack angle of the airfoil is 3°, and the Reynolds number is 2.14×10^6. To observe the influence of viscous effect, the NS equations and the Euler equations are solved by using the initial point distribution with the point spacing normal to the airfoil of 5×10^{-5} (Fig. 5) and 5×10^{-3}, respectively.

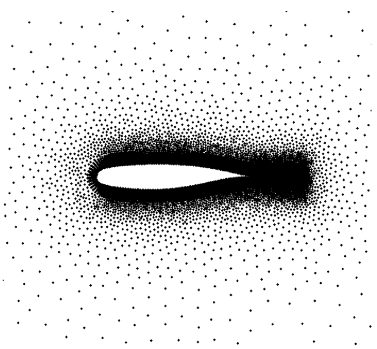

(a) Global view

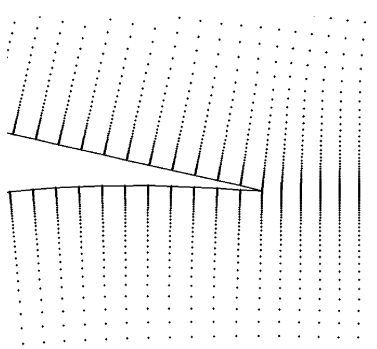

(b) Close-up view at trailing edge

Fig. 5 Point distribution around NLR7301 airfoil

Fig. 6 shows the stream lines when the trailing-edge flaps at the angle: $\delta(t)=1.0°$. There is a separate vortex at the upper surface of the trailing-edge. Figs. (7-9) show the obtained distribution of different parts of the unsteady pressure coefficient. The pressure distributions obtained from the Euler equations do not agree well with the experimental data[15], while those obtained from the NS equations concerning the viscous

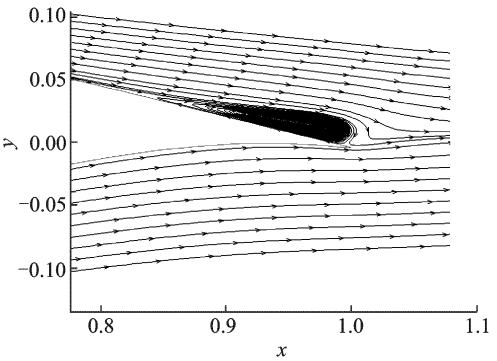

Fig. 6 Stream lines near trailing-edge

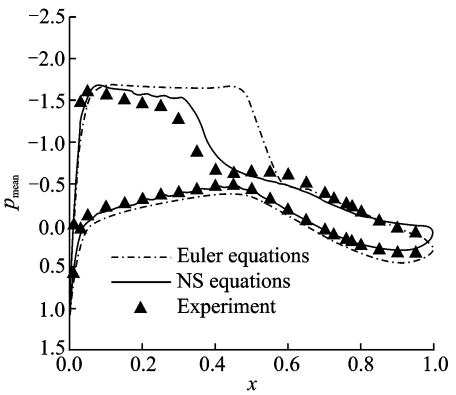

Fig. 7 Distribution of mean part of p

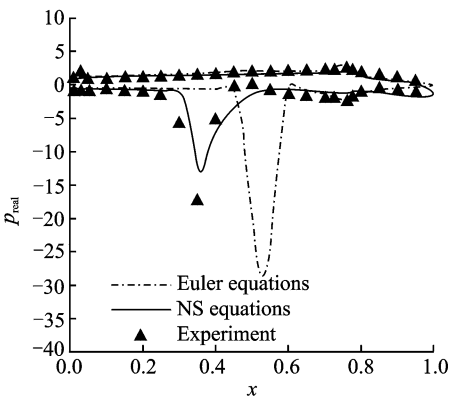

Fig. 8 Distribution of real part of p

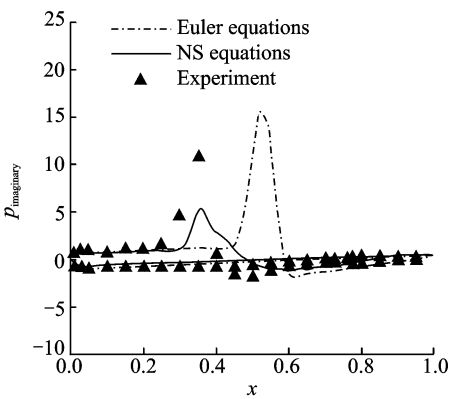

Fig. 9 Distribution of imaginary part of p

effect are much more close to the experimental data. Therefore, the NS equations are more suitable to solve this case. In addition, if laminar NS is applied, the solver can not even converge at every time step because the Reynolds number is as large as 2.14×10^6. Thus the effect of turbulence should be taken into account.

4.3 Dynamic stall on pitching NACA0012 airfoil

In this case, a NACA0012 airfoil is pitching at 25% of the chord with the attack angle: $\alpha(t)=6.25°+8.5°\sin(\omega t)$, and the reduced frequency $k=\omega c/2U_\infty=0.075$ where c represents the chord length and U_∞ the free stream velocity. The free stream Mach number is 0.4, and the Reynolds number is 3.4×10^6.

Numerical results are obtained by solving the NS equations and the initial point distribution is shown in Fig. 2. Fig. 10 presents the stream lines when the instantaneous attack angles are 14.75° (maximum angle) and −2.25°(minimum angle). In Fig. 10, when the instantaneous attack angle is 14.75°, there are three vortexes near the upper surface, while the stream flows along the surface smoothly when the instantaneous attack angle is −2.5°. In the whole cycle of the pitching, the flow features has a large range of change. Figs. (11-12) show the unsteady lift and moment coefficients versus the instantaneous attack angle respectively. Numerical prediction of the present gridless method are compared with the experimental data[15] and the results in Ref. [16], which achieves good agreement.

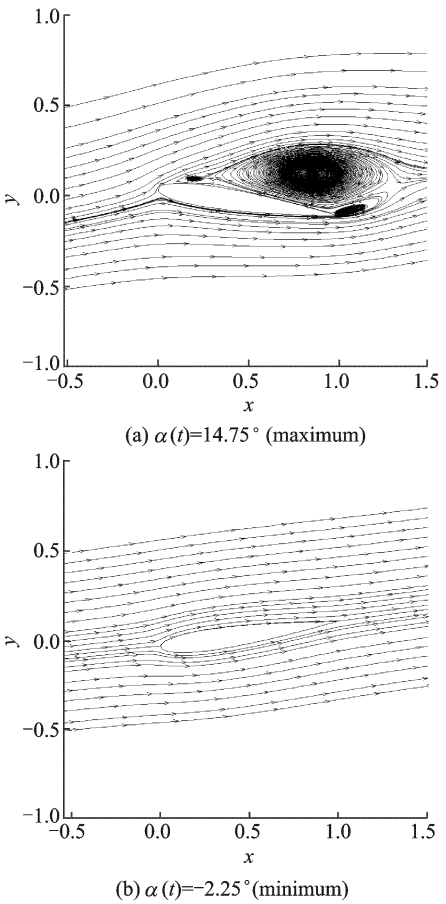

Fig. 10 Stream lines at different angles of attack

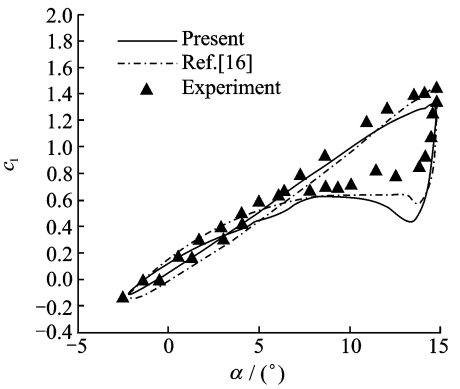

Fig. 11 Lift coefficient versus angle of attack

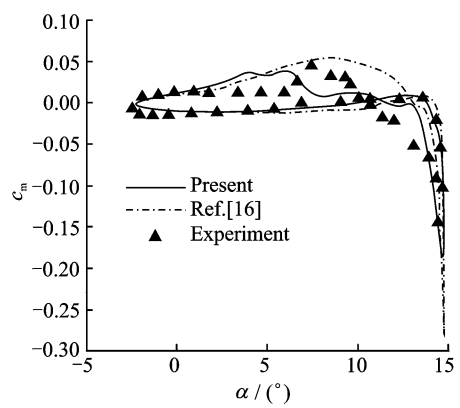

Fig. 12 Moment coefficient versus angle of attack

5 CONCLUSION

With concerning point distribution in an isotropic or anisotropic way, gridless method is successfully implemented for the NS equations. The verified numerical results show that the moving technique of clouds of points based on the attenuation law of disturbed motion can be easily applied for two-dimensional unsteady viscous flows involving moving boundaries. To simulate the unsteady flows involving large-scale moving

boundaries, some modifications including the reconstruction of the structure of some clouds are required, and the relevant research is in progress.

References:

[1] Batina J T. A gridless Euler/Navier-Stokes solution algorithm for complex aircraft applications[R]. AIAA 93-0333, 1993.

[2] Chen H Q, Shu C. An efficient implicit mesh-free method to solve two-dimensioanl compressible euler equations [J]. International Journal of Modern Physics C, 2005,16(3):439-454.

[3] Katz A, Jameson A. Edge-based meshless methods for compressible flow simulations[R]. AIAA 2008-699, 2008.

[4] Morinishi K. Gridless type solver-generalized finite difference method [J]. Notes on Numerical Fluid Mechanics, 2001,78:43-58.

[5] Kirshman D J, Liu F. Flutter prediction by an Euler method on non-moving Cartesian grids with gridless boundary conditions[J]. Computers & Fluids, 2006, 35:571-586.

[6] Wang G, Sun Y, Ye Z. Gridless solution method for two-dimensional nsteady flow[J]. Chinese Journal of Aeronautics, 2005,18(1):8-14.

[7] Wang H, Chen H, Ma Z, et al. Gridless method for solving moving boundary problems and its dynamic cloud points[J]. Journal of Nanjing University of Aeronautics & Astronautics, 2009,41(3):296-231. (in Chinese)

[8] Guo T. Transonic unsteady aerodynamics and flutter computations for complex assemblies[D]. Nanjing: College of Aerospace Engineering, Nanjing University of Aeronautics and Astronautics, 2006. (in Chinese)

[9] Spalart P R, Allmaras S R. A one-equation turbulence model for aerodynamic flows[R]. AIAA-92-0439, 1992.

[10] Pirzadeh S. Three-dimensional unstructured viscous grids by the advancing-layers method[J]. AIAA Journal, 1996,34(1):43-49.

[11] Weatherill N P. Delaunay triangulation in computational fluid dynamics[J]. Computers & Mathematics with Applications, 1992,24(5):129-150.

[12] Lu Z. Generation of dynamic grids and computation of unsteady transonic flows around assemblies[J]. Chinese Journal of Aeronautics, 2001,14(1):1-5.

[13] Blazek J. Computational fluid dynamics: Principles and Applications[M]. Amsterdam: Elsevier Science Ltd publisher, 2001:171-173.

[14] Thibert J J, Granjacques M, Ohman L H. NACA0012 Airfoil[R]. AGARD AR 138, 1979.

[15] Lambourne N C, Landon R H, Zwaan R J, et al. Compendium of unsteady aerodynamic measurements [R]. AGARD Report 702, 1982.

[16] Kerho M. Adaptive airfoil dynamic stall control[R]. AIAA 2005-1365, 2005.

用于非定常粘性流动计算的无网格算法

蒲赛虎 陈红全

(南京航空航天大学航空宇航学院,南京,210016,中国)

摘要:把无网格算法发展用于求解涉及动边界的非定常粘性流动问题。在处理粘性流动的布点问题时,通过在远离物面的区域采用无粘流动计算时所用的各向同性点云,而在物面附近引入各向异性点云,从而在保证物面法线方向布点较密以准确模拟边界层的同时,有效控制了布点总量,减少了计算时间。对于动边界问题,本文在上述方法获得的初始布点的基础上,采用基于扰动衰减规律的点云移动技术,快速得到物面运动到其他位置时流场求解所需点云。在所获得的点云上,采用一种带权系数的二次极小曲面逼近方法来离散Navier-Stokes方程的空间导数,权系数的引入使得流场求解时对各向同性点云和各向异性点云无需分开考虑,而是采用统一的求解方法,从而简化了编程求解。用发展的无网格算法,结合Navier-Stokes方程求解双时间推进方法,并耦合Spalart-Allmaras湍流模型,先成功地模拟出NLR7301翼型后缘摆动诱发的非定常流,并通过与实验比较,验证了本方法.接着进行了NACA0012失速模拟,给出了动态失速过程,展示出用本文方法处理复杂动边界问题的效果。

关键词:无网格算法;点云;Navier-Stokes方程;非定常流动;粘性流动

中图分类号:V211.3

(Executive editor: Zhang Bei)

基金项目:国家自然科学基金(10372043,11172134)资助项目;江苏省普通高校研究生科研创新计划(CXZZ11_0192)资助项目。